Polarization Modulation in Ferroelectric Organic Field-Effect Transistors

A. Laudari,[1] A. R. Mazza,[1] A. Daykin,[1] S. Khanra,[1] K. Ghosh,[2] F. Cummings,[3] T. Muller,[3] P.F. Miceli,[1] and S. Guha[1,*]

[1] *Department of Physics and Astronomy, University of Missouri, Columbia, Missouri 65211, USA*
[2] *Department of Physics, Astronomy, and Materials Science, Missouri State University, Springfield, MO 65897, USA*
[3] *Department of Physics, University of the Western Cape, Robert Sobukwe Road, Bellville 7535, South Africa*

(Received 29 October 2017; revised manuscript received 10 February 2018; published 16 July 2018)

The polarization modulation effect of the gate dielectric on the performance of metal-oxide-semiconductor field-effect transistors has been investigated for more than a decade. However, there are no comparable studies in the area of organic field-effect transistors (FETs) using polymer ferroelectric dielectrics, where the effect of polarization rotation by 90° is examined on the FET characteristics. We demonstrate the effect of polarization rotation in a relaxor ferroelectric dielectric, poly(vinylidene fluoride trifluorethylene) (PVDF-TrFE), on the performance of small-molecule-based organic FETs. The subthreshold swing and other transistor parameters in organic FETs can be controlled in a reversible fashion by switching the polarization direction in the PVDF-TrFE layer. X-ray diffraction and electron microscopy images from PVDF-TrFE reveal changes in the ferroelectric phase and domain size, respectively, upon rotating the external electric field by 90°. The structural changes corroborate density-functional-theoretical studies of an oligomer of the ferroelectric molecule in the presence of an applied electric field. The strategies enumerated here for polarization orientation of the polymer ferroelectric dielectric are applicable for a wide range of polymeric and organic transistors.

DOI: 10.1103/PhysRevApplied.10.014011

I. INTRODUCTION

Organic ferroelectrics are playing an increasingly important role in flexible memory devices, actuators, transducers, and wearable electronics [1–3]. In addition to nonvolatile memory devices [4–6], poly(vinylidene fluoride)- (PVDF-) based ferroelectric polymer and its copolymers have been used for pressure sensing [7,8] and organic photovoltaic devices [9]. The vast range of work has utilized PVDF and its copolymers as a gate dielectric in organic field-effect transistors (FETs) [10–13]. Electronic polarization effects, which may be either short- or long-range lattice fluctuations, play an inherent role in FET transport. The dynamic coupling of the charge carriers to the electronic polarization at the semiconductor-dielectric interface is manifested as Fröhlich polarons when the gate dielectric is sufficiently polar [14,15]. Interactions at the interface result in a renormalization of the transfer integral for the transport process, altering carrier mobilities. Inhomogeneous strain at the semiconductor-dielectric interface due to mismatch between the coefficient of thermal expansion has been further seen to dictate the hopping nature versus bandlike transport in organic FETs [16].

A juxtaposition of ferroelectric polymers and ferroelectric oxides shows metal-oxide-semiconductor field-effect transistors (MOSFETs) have greatly benefited from the intrinsic spontaneous electric polarization of ferroelectric oxides. Polarization modulation in ferroelectric oxides has enabled fast switching and low-power operation in MOSFETs [17,18]. The spontaneous electric polarization of ferroelectric oxides not only controls the channel conductance but may be further reoriented by the application of an external electric field [19,20]. Although the polarization-distribution effect of the ferroelectric oxide on the channel current-gate voltage has been considered in MOSFETs [21,22], there are no such parallel studies on polymer ferroelectric FETs, especially where the effect of rotating the polarization direction by 90° on FET performance has been examined. As stated earlier, there are several works that have utilized polymer ferroelectrics in organic FETs for elucidating basic charge-transport properties or in memory applications. The list is exhaustive and we only cite a few representative works here.

The discovery of the piezoelectric effect in PVDF dates back to the pioneering work by Kawai [23]. Much of the structural and ferroelectric properties of PVDF and its copolymers with trifluorethylene (TrFE) were determined in the early 1980s [24–26]. PVDF is a relaxor ferroelectric

*guhas@missouri.edu

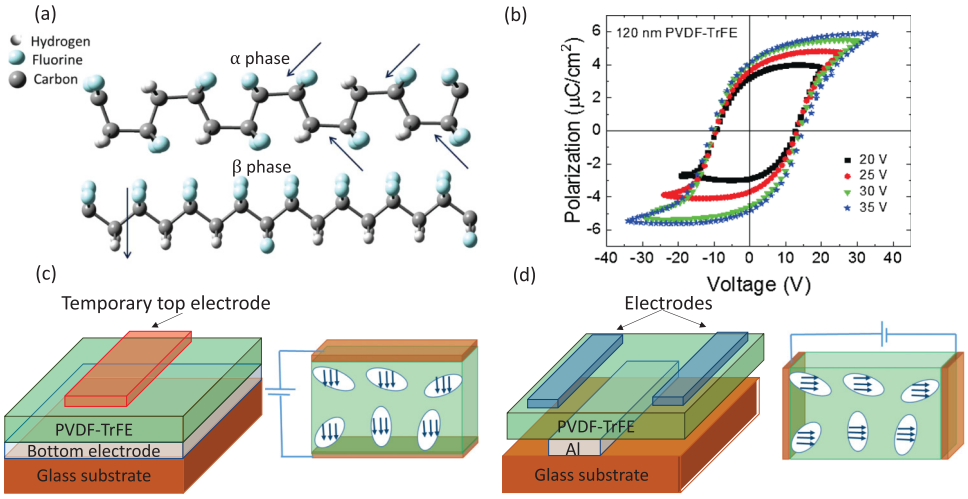

FIG. 1. Chemical structure and poling of PVDF-TrFE films. (a) Schematic representation of the chain conformation for the α and β phases of PVDF-TrFE. Arrows denote the direction of the dipole moment. (b) Polarization versus voltage hysteresis curves for Al-PVDF-TrFE-Au capacitors at 1 kHz. (c),(d) Schematic of vertical and lateral poling of PVDF-TrFE, respectively. Arrows denote the polarization direction in the crystalline phases of the ferroelectric slab after poling.

with dipolar domains embedded in an amorphous matrix. PVDF exists at least in four different phases: α, β, γ, and δ, of which the α and β phases are the most predominant [26]. The α belongs to the paraelectric phase with a conformation of *trans-gauche* (TG+TG−) and β PVDF is the all-*trans* configuration (TTTT) in which the bonds on each successive carbon are 180° away from the previous ones, as shown in Fig. 1(a). The ferroelectric properties of β PVDF arise from the differing electronegativity of hydrogen and fluorine, giving rise to a dipole for each molecule oriented perpendicular to the polymer chain. PVDF films are not ferroelectric upon spincasting; they require additional measures such as stretching of the polymer or controlled heating of the film to ensure the all-*trans* configuration [27]. The advantage of the copolymer, PVDF-TrFE, is that it is ferroelectric after directly processing the film. The ferroelectricity in the copolymer arises from a balance of short-range van der Waals interaction due to the alignment of molecular dipoles and the long-range dipole-dipole interactions between the chains.

Unlike MOSFETs, which operate in the inversion region, organic FETs typically work in the accumulation mode, where charges are injected by the source and drain contacts and the channel region is formed at the interface of the organic semiconductor and the dielectric layer. Over the last decade, the field of organic FETs has seen an increasing usage in polymer dielectric materials and a progressively lower dependence on traditional oxide dielectrics [28], which has resulted in a quest for gate dielectrics that are hydrophobic and free from charge-trapping groups. PVDF-based dielectrics have provided a tuning knob to monitor transport in FETs as the dielectric constant κ changes with temperature [29,30]. In PVDF-TrFE, κ increases by almost a factor of 5 from 200 K till its ferroelectric-paraelectric transition temperature at 390 K. Since the electronic polarization directly impacts FET transport properties, temperature-dependent transport from PVDF-TrFE-based organic FETs shed light on the mechanism of polarization fluctuation driven transport in polymeric and small-molecule-based organic FETs [29–31]. Time-resolved optical second-harmonic-generation techniques and modulation spectroscopy such as charge modulation reflectance from PVDF-based organic FETs have allowed the visualization of electric fields in the semiconducting layer [32,33]. There have been some studies on improving switching speeds and carrier mobilities in PVDF-TrFE-based polymeric FETs by electric field-induced modification of the ferroelectric dielectric layer [34,35].

A recent theoretical work shows the effect of polarization rotation on the performance of MOSFETs using $BaTiO_3$ as the gate insulator [36]. Polarization rotation changes the surface potential of the silicon substrate, resulting in a subthreshold swing (SS) lower than 60 mV/decade by a judicious choice of the thickness of the gate dielectric layer. It is seen that polarization rotation (from out-of-plane to in-plane) offers significant advantages over polarization inversion in the $BaTiO_3$ layer. Spontaneous polarization during the reorientation increases the screening charge accumulation in the MOSFET channel, resulting in low SS. Although the SS of FETs based on polycrystalline organic films have now paralleled those of MOSFETs with values close to 90 mV/decade [37,38], they usually involve a self-assembled monolayer on high-quality oxide dielectrics such as AlO_x. In single-crystal rubrene FETs, the disorder is significantly reduced with interface trap densities similar to that in silicon transistors, and SS values of 65 mV/decade have been achieved [39]. A question that arises is whether polarization reorientation in a polymer ferroelectric dielectric is an effective mechanism for improving SS and other transistor parameters in organic FETs? Specifically, we are interested in changes in SS and other FET parameters by rotating the polarization direction of the dielectric by 90°. Polarization rotation is different from polarization inversion, which in principle may be achieved by sweeping the gate from high

negative to positive voltages in ferroelectric organic FETs. Such inversion effects have benefits in changing the on-off ratio for memory application [40].

By using two different organic molecules: Dinaphtho [2,3-b:2′,3′-f]thieno[3,2-b]thiophene (DNTT) and pentacene, and a small-molecule solution processable semiconductor, 6,13-bis(triisopropylsilylethynyl)pentacene (TIPS-pentacene) along with as-is and poled PVDF-TrFE as the gate dielectric, in top-contact bottom-gate FET architectures, carrier transport is investigated. Prior to depositing the organic semiconductor, the ferroelectric film is either vertically or horizontally poled by applying an external electric field while heating the polymer just above its ferroelectric-paraelectric transition temperature at 130°C, which is known to increase the degree of crystallinity [41]. The presence of additional lateral electrodes with vertically poled FETs facilitates the application of a lateral electric field, which helps monitor transistor properties as a function of reorientation of the polarization direction by 90° in the dielectric medium. Since we investigate *p*-type transport, the poling direction is appropriately chosen. The FETs with the vertically poled PVDF-TrFE film perform the best with the lowest value of SS. As a lateral electric field is applied to the vertically poled FETs, the transistor characteristics are seen to degrade. The phenomenon is reversible; by applying a lateral field in the opposite direction, the transistor properties recover. The FETs operate at lower voltages compared to the coercive voltage of the PVDF-TrFE layer, ensuring that the changes observed in the FET properties arise from external poling conditions. The poling field controls the microstructure of PVDF-TrFE, which is inferred from x-ray diffraction (XRD) and electron microscopy images. Density-functional-theory (DFT) studies from a monomer unit embedded in a dielectric medium under the application of both vertical and horizontal electric fields shed light on the changes in the net dipole moment and structure (deviation from the all-*trans* phase) of the molecule. This study highlights new design principles for organic FETs in lowering SS and enhancing transport properties by orienting the polarization direction by 90° in the ferroelectric dielectric layer.

II. EXPERIMENTAL DETAILS

A. Materials

The materials used are as follows: organic semiconductors dinaphtho[2,3-b:2′,3′-f]thieno[3,2-b]thiophene (DNTT) and 6,13-bis(triisopropylsilylethynyl)pentacene (TIPS pentacene) are procured from Sigma Aldrich Inc, and pentacene is procured from Tokyo Chemical Industry. All semiconductors are used without any purification. The dielectric copolymer, poly(vinylidene fluoride trifluoroethylene (PVDF-TrFE) (75:25) is obtained from Measurement Specialties Inc. The solvent *N*,*N*-dimethylformamide is procured from Sigma Aldrich. Glass substrates and Si^{2+} wafers are obtained from Fisher Scientific.

B. Poling of PVDF-TrFE films and device fabrication

60 nm aluminum film is deposited on clean glass substrates via thermal evaporation for the bottom electrode. PVDF-TrFE is dissolved in the solvent N, N-dimethylformamide (50 mg/ml) (DMF). This dielectric solution is then spin casted on top of the Al-coated glass at a spin speed of 1600 rpm for 60 sec and heated at 70°C for 10 minutes to remove the solvent residue. The PVDF-TrFE films are then annealed at 135°C for half an hour for further enhancement of the β phase of the copolymer. PVDF-TrFE films are vertically poled by applying an electric field of ∼100 MV/m during the crystallization process. A temporary electrode is prepared by depositing 300 nm of Al on a glass slide. Electrical contacts are made and the slide is placed (with the Al strip facing down) on top of the PVDF-TrFE film, as shown in Fig. 1(c). A 50-g weight is added on top to ensure a uniform contact of the top electrode with the ferroelectric surface. The field is applied between the temporary top electrode and the bottom Al electrode. The field is on while the film is allowed to slow cool for half an hour. Two aluminum strips, 2.0 mm apart, are deposited on a few films by the shadow mask method as lateral poling electrodes. We note that the lateral electrodes are deposited on top of the PVDF-TrFE film whereas the gate electrode is placed under the dielectric layer. Additionally, there is no overlap between the top lateral electrodes and the gate electrode (as shown in Fig. 1(d) and Fig. S1 [42]). During lateral poling, the voltage is only applied to the lateral electrodes. Hence, the electric field should be uniform during lateral poling. About 0.1 MV/m lateral field is applied to these films for 15 minutes at 135°C. Lateral poling electrodes are also deposited on vertically poled films to access lateral poling during the device characterization. For metal-insulator-metal (*M*-*I*-*M*) capacitors, unpoled, vertically poled, and laterally poled PVDF-TrFE films on Al-coated glass are followed by 60 nm aluminum or gold through a shadow mask to complete the MIM structure.

Unpoled, vertically poled, and laterally poled PVDF-TrFE films on Al-coated glass are followed by 30 nm thermally deposited DNTT (0.3 Å/s, 10^{-5} mbar). Finally, 50 nm source and drain gold electrodes are deposited through a shadow mask. These masks also allow the evaporation of Au in small circular regions for metal-insulator-semiconductor (*M*-*I*-*S*) structures. Similar FETs are fabricated by evaporation of pentacene. The dielectric film thicknesses are inferred from capacitance measurements of MIM devices and are further confirmed with a reflectometer and a profilometer. TIPS pentacene FETs are also fabricated by drop casting a solution of TIPS pentacene (in anhydrous toluene) on PVDF-TrFE films

(vertically poled and unpoled), as outlined in Ref. [31], before depositing the top source and drain Au electrodes. For XRD and SEM measurements, the PVDF-TrFE films are prepared in a similar fashion as in MIM and FETs, except the thickness is higher (∼800 nm), and the films are grown on Si^{2+} substrates for XRD.

C. Characterization

The capacitance measurements from MIM and MIS structures are carried out with an HP 4284A precision *LCR* meter. During the measurements, a dc voltage is applied to the capacitor with a small ac-voltage signal superimposed upon the dc signal. Capacitance is recorded as the dc bias is swept. The magnitude of the ac signal is 200 mV and the frequency of the signal is 5 kHz for all measurements. The dc signal is swept from both positive to negative bias and vice versa. Variation of capacitance with frequency in a range of 10 Hz to 1 MHz is also measured; stable capacitance with minimum leakage is obtained at 5 kHz. For the vertically poled film, lateral fields (0.025 MV/m to 0.1 MV/m) are applied for 15 minutes and the capacitance measurements are repeated after each lateral poling. Polarization measurements from unpoled MIM structures are performed at 1 kHz using a Sawyer-Tower circuit.

Room-temperature dc current-voltage (*I*-*V*) measurements from FETs are performed using two source meters, Keithley 2400 and Keithley 236, using a customized LabVIEW program. The effect of lateral fields on vertically poled films is explored by applying lateral fields (0.025 MV/m to 0.1 MV/m) for 15 minutes and repeating the FET characterization after each lateral poling.

XRD data are collected using a Rigaku R-Axis IV image plate (IP) area detector and a Rigaku RU-300 x-ray generator with Cu *K* radiation (0.15417 8 nm) from a focusing multilayer mirror optic. The IP is fixed at a sample-detector distance of ∼75 mm with the plane of the IP oriented perpendicular to the direct beam. Unpoled, vertically poled, laterally poled, and blank silicon samples are all measured at an incident angle of 4.5° with respect to the plane of the substrate. Two-dimensional powder diffraction rings measured on the IP are integrated azimuthally in order to obtain a one-dimensional intensity profile. Samples are exposed to x rays for 8 minutes using the same generator power (35 kV, 80 mA).

Low-voltage secondary-electron micrographs of the film surface morphology are collected with a Zeiss Auriga field-emission gun-scanning electron microscope (FEG SEM) at an accelerating voltage of 1 keV. The thin films remained uncoated, with the surfaces cleaned in the microscope chamber using a nonreactive nitrogen plasma (XEI Scientific Evactron decontaminator) for 10 minutes. This ensured effective removal of hydrocarbon contamination on the thin-film surface and minimal radiation damage during analysis.

D. Theory

DFT calculations are performed using GAUSSIAN09 [43]. We employ the Becke's three-parameter hybrid (B3LYP) functional combined with the 6-311++g (2d,p) basis set for geometry optimization and obtaining the dipole moment. One unit of the PVDF-TrFE (3:1) molecule is optimized in the presence of DMF solvent (with no external field). The optimized molecule is further optimized with varying applied electric fields in the solvent environment. First, an electric field is applied perpendicular to the chain axis of the molecule, which is increased in certain increments; the molecule is optimized at each field, using the configuration of the prior step. After applying the maximum vertical electric field (without destroying the molecule), a lateral field along the axis of the molecule is applied. This field is again varied and the molecule is optimized at each step. A few cases of reversing the direction of the lateral field are also studied.

III. RESULTS AND DISCUSSIONS

A. Polarization of PVDF-TrFE

The 75:25 PVDF-TrFE used in this work ensures >50% crystallinity. Unlike ferroelectric oxides such as $BaTiO_3$, which have a relatively large spontaneous polarization (∼0.26 C/m^2), the spontaneous polarization in PVDF and its copolymers are ∼0.05 C/m^2 for 50% crystalline samples [44]. Additionally, high fields (> 10^6 V/cm) are needed to reverse the polarization at room temperature; only a partial reversal may occur at lower electric fields [45]. Figure 1(b) shows typical polarization versus voltage loops from a metal–PVDF-TrFE–metal capacitor. These measurements are from a 120-nm thick dielectric layer, similar to the thickness used in FETs. Such PVDF-TrFE film thicknesses in organic FETs result in operating voltages of 2 V. The low operating voltage in FET architectures implies that a reversal or rotation of polarization in the dielectric medium does not occur during the normal operation of the FET. Hence, external poling provides an independent tool to orient and reorient the polarization direction in the dielectric medium by 90°, and allows the subsequent FET properties to be tracked.

Figures 1(c) and 1(d) show the strategies for orienting the polarization direction. Vertical poling is achieved as explained in Sec. II B. For lateral poling, two sets of Al electrodes, which are 2.0 mm apart, are evaporated. In such structures, the electric field during poling is three orders of magnitude smaller than in vertical poling. For some samples that are vertically poled, the lateral electrodes are evaporated for applying a lateral field in the FET architecture itself. Fig. S1 of the Supplemental Material [42] shows a schematic and an image of the FETs used in this work. Poling is achieved such that the net polarization [indicated

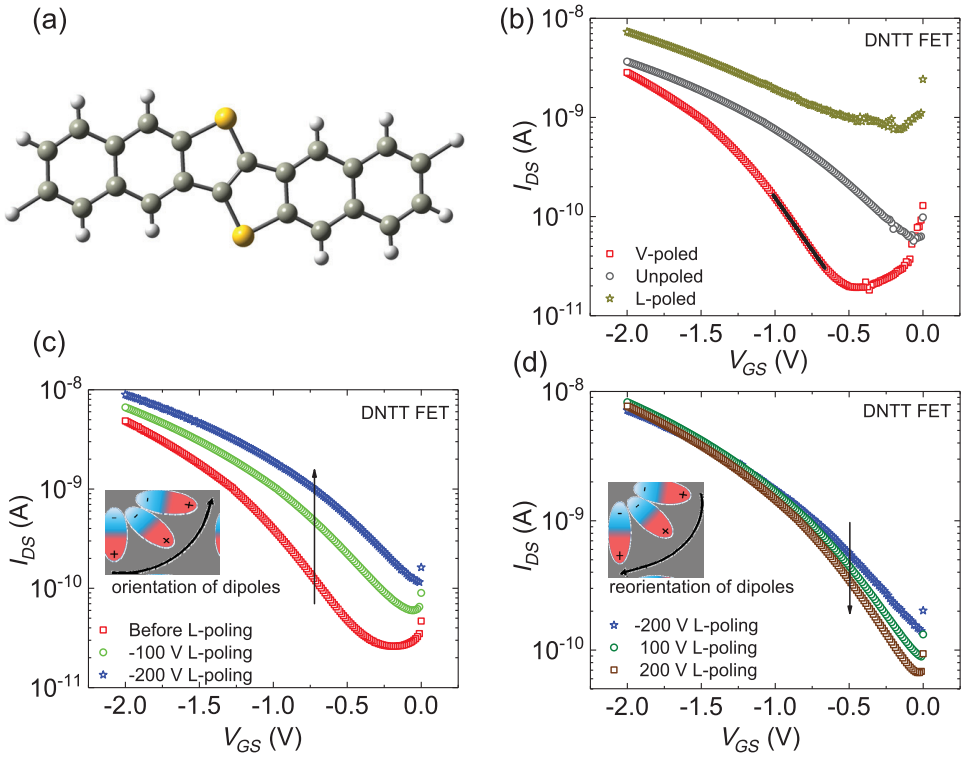

FIG. 2. Transfer characteristics of DNTT-based FETs. (a) Chemical structure of DNTT. (b) Transfer characteristics of DNTT FETs with V-poled, unpoled, and L-poled PVDF-TrFE. The black line depicts a linear fit to the subthreshold region. (c) Transfer characteristics of a vertically poled FET by applying various magnitudes of a lateral voltage. Green and blue curves depict devices where the lateral field is applied such that the polarization direction of the dielectric is oriented parallel to the external source-drain electric field. (d) Transfer curves of the same FET device shown in (c) after reversing the polarity of the lateral field, such that the polarization direction is oriented antiparallel to the source-drain electric field.

by the blue arrow in Figs. 1(c) and 1(d)] within the dielectric layer is parallel to the gate field and the source-drain field for vertical-(V) and lateral-(L) poled PVDF-TrFE films, respectively. Since p-type transport is probed, the gate field in the FET is directed vertically downwards.

B. Small-molecule FETs with poled and unpoled PVDF-TrFE

DNTT, a small-molecule organic semiconductor, is a highly π-extended heteroarene with six fused aromatic rings [chemical structure is shown in Fig. 2(a)]. It has good air stability and demonstrates high FET charge-carrier mobility $\sim$2 cm^2/V s when AlO_x with a self-assembled monolayer is used as the dielectric layer [46]. DNTT FETs are prepared on three different substrates with unpoled, V-poled, and L-poled PVDF-TrFE films. The film thickness of the dielectric and the semiconducting layer are identical for all three substrates. The output characteristics of the DNTT FETs with V-poled, unpoled, and L-poled PVDF-TrFE are shown in Fig. S2 [42]. The transfer characteristics of the three samples are shown in Fig. 2(b). These are all swept in the saturation region where the drain-source voltage (V_{DS}) is maintained at -2 V, and the gate voltage (V_{GS}) is varied. Device parameters such as carrier mobility, μ, on-off current ratio, and threshold ($V_{\rm th}$) are estimated using the standard saturation regime current-voltage characteristics: $I_{DS} = (\mu W C_O/2L)(V_{GS} - V_{\rm th})^2$, I_{DS} being the drain-source current, C_O is the dielectric capacitance per unit area, and W and L correspond to the channel width and length, respectively. By a linear fit to the saturation region of the square root of I_{DS} versus V_{GS}, μ is deduced. L varied between 50 and 125 μm for the FETs. The double linear plots of the transfer characteristics (saturation and linear region) for V-poled DNTT FET are shown in Fig. S4 with details on how μ is extracted. More than the changes in μ, the subthreshold swing and other FET parameters, as discussed below, vary with the poling condition; hence, we quote only the saturation mobilities. A recent work by Choi *et al.* [47] defines the reliability factor r for extracting carrier mobilities both in the saturation and linear regions of the transfer characteristics. The r factor is defined based on the ideal Shockley FET equations with $V_{\rm th} = 0$. Based on this definition, the r factor for $\mu_{\rm sat}$ (V-poled FET) is found to be $\sim$47%. We point out that for ferroelectric dielectrics the value of $V_{\rm th}$ can greatly vary, from being positive to negative, as discussed later. Hence, one cannot expect an ideal r factor of $\sim$100%.

The SS, which is expressed as $\{[\partial \log(I_{DS})]/\partial V_{GS}\}^{-1}$, varies for the three FETs. Using the subthreshold region ($V_{\rm th} \ll V_{GS} \ll V_{\rm on}$), SS is obtained. A representative linear fit (black line) for the V-poled device is shown in Fig. 2(b). We note that this fit just represents the subthreshold region used for obtaining SS; the carrier mobilities are obtained as outlined above. It may be more appropriate to compare the normalized equivalent of SS by taking into account the capacitance of the insulator ($SS_i = SS \times C_O$), as defined for single-crystal FETs [48]. The FET parameters including SS_i are tabulated in Table I. Several devices are tested. The FET with the V-poled PVDF-TrFE films shows the

TABLE I. Electrical parameters for DNTT and pentacene-based PVDF-TrFE FETs for different poling conditions of the dielectric. SS is the subthreshold swing and the normalized SS is defined in the text.

Semiconductor	Dielectric poling condition	SS (mV/dec)	Normalized SS (nF V/dec cm^2)	Mobility (10^{-3} cm^2/V s)
DNTT	V-poled	403 ± 5	37	11.3 ± 0.2
	Unpoled	1000 ± 8	62	6.0 ± 0.1
	L-poled	1700 ± 11	105	5.0 ± 0.1
Pentacene	V-poled	600 ± 4	55	2.9 ± 0.1
	Unpoled	1100 ± 7	68	1.6 ± 0.2
	L-poled	1140 ± 9	71	1.5 ± 0.1

lowest value of SS (and SS_i), and the highest value of μ. The L-poled FET performs worse than the unpoled device, which is an indication that there is some orientation of the dipoles in the vertical direction in unpoled PVDF-TrFE films. The contact resistance is obtained using the transmission-line method [49–51], and is similar for the three sets of FETs (see [42] for details).

Pentacene FETs with V-poled, unpoled, and L-poled PVDF-TrFE are also fabricated. The transfer curves (in the saturation region) are shown in Fig. S6 [42], and their SS, SS_i, and μ values are tabulated in Table I. The device performance trends are identical to DNTT FETs; the V-poled pentacene FET performs the best with the lowest value of SS and the highest value of μ. TIPS-pentacene FETs are also fabricated with V-poled and unpoled PVDF-TrFE; one of the lowest values of SS (<200 mV/dec) is observed for V-poled PVDF-TrFE TIPS-pentacene FET (Fig. S7) [42].

The general trend is that V-poled PVDF-TrFE FETs show the lowest off current with improved SS. An improvement in carrier mobility is also observed for all V-poled devices. Since the direction of polarization (**P**) in V-poled PVDF-TrFE film is in the same direction as the gate electric field, it enhances the screening charge accumulation in the channel region improving transport, resulting in a lower value of SS. Concomitantly, the accumulation capacitance in a MIS diode is seen to increase for the V-poled film. Capacitance-voltage (C-V) sweeps from DNTT and pentacene MIS structures (with unpoled and V-poled PVDF-TrFE films) are shown in Figs. S3 and S6 [42]. In both cases, the capacitance in the accumulation region is higher when the PVDF-TrFE film is V-poled compared to the unpoled case. The change in capacitance is also seen in MIM structures with different poling conditions of the insulator, as discussed later.

A question that arises is whether the FET properties are tunable by changing the polarization direction of the dielectric medium. The V-poled FETs are incorporated with lateral electrodes (at a separation of ~2 mm). The lateral electric field is applied for 15 minutes and its magnitude is in the range of 10^4–10^5 V/m. Figure 2(c) shows the transfer curves measured after the application of a lateral electric field (with varying magnitude) to the V-poled sample. The direction of **P** (with the lateral field) is in the same direction of the source-drain electric field ($\mathbf{E}_{DS}$). As the vertical polarization is reoriented in the horizontal direction, it results in degradation of the FET properties, which is seen in the transfer curves. The tabulated values of SS and μ are shown in Table II. The normalized SS also show the same trend; hence, we do not explicitly quote the values here. We note that the DNTT V-poled FETs in Table I are a different batch compared to the V-poled DNTT FET shown in Table II. The initial L-poled FET has a larger SS compared to L-poling a V-poled FET device. Since the original V-poled film is already crystallized, applying only a lateral field may not have the same effect as applying a lateral field during crystallization.

TABLE II. FET parameters for a vertically poled PVDF-TrFE film using DNTT as the organic semiconductor. Lateral electric field is applied in the direction of $\mathbf{E}_{DS}$, and then the polarity is reversed.

Dielectric poling condition	Subthreshold swing (mV/dec)	Threshold voltage (V)	Mobility (10^{-3} cm^2/V s)
Vertical	530 ± 2	−0.78	11.00
Lateral (−50 V)	580 ± 3	−0.47	10.00
Lateral (−100 V)	650 ± 3	−0.40	9.40
Lateral (−150 V)	660 ± 5	−0.27	9.20
Lateral (−200 V)	700 ± 7	−0.22	9.00
Polarity reversed			
Lateral (100 V)	650 ± 4	−0.30	8.30
Lateral (200 V)	580 ± 3	−0.33	9.40

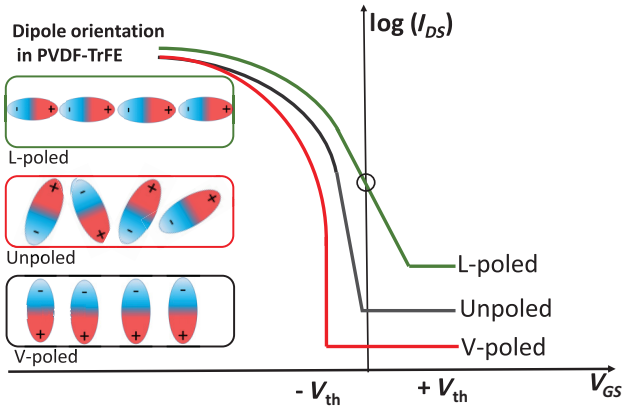

FIG. 3. Schematic transfer curves of PVDF-TrFE-based FETs for different poling conditions. V_{th} may be positive or negative. A slightly positive V_{th} for the L-poled FET results in a higher current at zero gate bias condition (depicted by the circle). The dipole orientation in PVDF-TrFE with poling conditions are also shown.

After the FET is L-poled to $\sim 10^5$ V/m (-200 V), the direction of L-poling is reversed [Fig. 2(d)]. The FET properties are seen to recover (also shown in Table II). The L-poling of a V-poled sample, thus, serves as a tuning knob to reorient the polarization by 90°. In order to gain insight into the interface potential for different poling conditions, Grünewald's method [52], which has been extensively used for estimating the trap density of states, [53,54] is used. By determining the dependence of I_{DS} on the electric field due to V_{GS}, the gate-dependent dielectric-semiconductor interface potential $V_0 = V_0(U_g)$ is determined from:

$$\exp\left(\frac{eV_0}{kT}\right) - \frac{eV_0}{kT} - 1 = \frac{e}{kT}\frac{\epsilon_i d}{\epsilon_s l \sigma_0}\left[U_g \sigma(U_g) - \int_0^{U_g} \sigma(\tilde{U}_g) d\tilde{U}_g\right], \quad (1)$$

where e, k, and T are the elementary charge, the Boltzmann constant, and the absolute temperature, respectively; $U_g = |V_{GS} - V_{FB}|$ and V_{FB} is the flat-band voltage; $\sigma(U_g) = (L/W)(I_{DS}/V_{DS})$ is the field-dependent conductivity, and σ_0 is the conductivity at $U_g = 0$; ϵ_i and ϵ_s are the dielectric constants of the insulator and the semiconductor. For each gate voltage, Eq. (1) is numerically evaluated using the measured field-effect conductivity. V_{FB} is assumed to be the onset gate voltage of the device. The interface potential as a function of U_g is plotted in Fig. S8 [42] for the V-poled sample and after L-poling it at -50 and -200 V. There is a slight increase in this potential upon L-poling the device, which agrees with an increase in SS. By rewriting SS as $[\partial V_{GS}/\partial V_0][\partial V_0/\partial \log(I_{DS})]$, the changes in SS may be attributed to an increase in the first term. Further, the total hole density, $p(V_0)$, is dependent on the interface potential [$p(V_0) \propto (dV_0/dU_g)^{-1}$]. In the example shown in Fig. S8 [42], it is seen that upon L-poling the V-poled film, the hole density decreases. This decrease suggests more trapping upon L-poling and a reduction in the carrier mobility.

We note that the operating voltages of the FETs are well below the coercive fields; thus no spontaneous polarization inversion is expected. The differences in the V-poled, unpoled, and L-poled FETs may be further understood in terms of V_{th}, as shown schematically in Fig. 3. The L-poled FET has a slightly positive V_{th} [Fig. 2(b)]. Hence, at zero gate voltage there is some current flowing between the source and drain electrodes, reducing both the on-off ratio and SS compared to the V-poled or unpoled devices. Although the effect of L-poling the V-poled device is not as dramatic as the initial L-poled sample, the trends are similar; V_{th} becomes less negative with L-poling (Table II). It is worth pointing out that charge modulation reflectance measurements from pentacene ferroelectric FETs suggest a minority carrier injection near the source and drain electrodes, when the polarization direction is inverted (positively polarized at the interface) [33].

In addition to the changes in the interface potential with different poling conditions, one may ask the following questions in order to understand the dependence of the polarization rotation on the FET properties: does the microstructure of the PVDF-TrFE film change when it is V- or L-poled? Does the thickness of the dielectric medium play a role in the polarization reorientation process? Before looking at the structural changes in PVDF-TrFE upon poling, we comment on the C-V measurements from MIM structures. These measurements serve as an independent tool to understand how the charge accumulation at the interface may be enhanced by orienting the polarization.

C. Capacitance-voltage characteristics of PVDF-TrFE MIM capacitors

Figure 4(a) shows the C-V characteristics from Al–PVDF-TrFE–Au MIM structures for unpoled, V-poled, and L-poled films, measured at 5 kHz. All films had similar dielectric layer thicknesses $\sim$120 nm. As expected from ferroelectric capacitors, PVDF-TrFE-based MIM capacitors exhibit a hysteresis with butterfly loops due to polarization reversal [55,56]. The C-V hysteresis indicates that the capacitance changes from an accumulation state to an inversion state. Clear differences are observed between the V-poled, and the unpoled and L-poled films. The V-poled film has the highest value of capacitance; the L-poled film shows the highest asymmetry in the loop. The polarization switching occurs at the coercive voltage (V_c); for the unpoled film $V_c \sim 7$ V, similar to what is seen in the polarization versus voltage loop (Fig. 1). The dissipation factor, tanδ, is reasonably low ($\sim$0.03) between ± 15 V

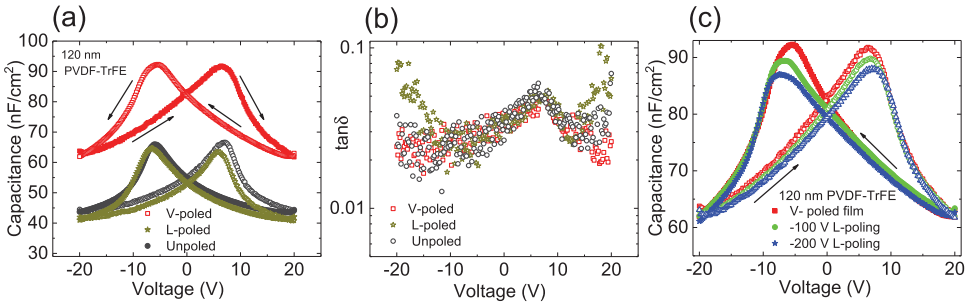

FIG. 4. Capacitance-voltage characteristics of PVDF-TrFE MIM capacitors. (a) Capacitance versus voltage curves for V-poled, L-poled, and unpoled PVDF-TrFE films. Arrows show the direction of the applied voltage. (b) Corresponding tanδ values from the three films. (c) Capacitance versus voltage curves after L-poling of a V-poled film.

[Fig. 4(b)]. The *C-V* measurements are further carried out from the V-poled MIM capacitor by applying a lateral voltage, shown in Fig. 4(c). With an increase in the L-poling voltage, the overall accumulation capacitance decreases. These observations corroborate the FET characteristics; the SS value decreases with an increase in L-poling of the V-poled device [Fig. 2(b)].

Polarization-rotation studies are further conducted on thinner PVDF-TrFE (30 nm) DNTT FETs, details of which are provided in Ref. [42]. Results from the thinner PVDF-TrFE films confirm two aspects. First, the operating voltages can be further reduced, well below −2 V, improving the overall transport properties in DNTT FETs. Second, it confirms that ∼120 nm thickness is within the critical regime where polarization rotation is achievable, similar to the 30 nm devices.

Irrespective of the organic semiconductor layer, our results show that the polarization orientation in the polymer ferroelectric layer directly impacts FET performance. In particular, SS of the FET transfer characteristics may be lowered by orienting **P** in a direction parallel to the applied gate electric field. This agrees well with some of the highest switching times that have been observed for polymer ferroelectric FETs when the interface layer is prebiased in the perpendicular direction [34]. In order to understand how the microstructure affects the overall polarization in the ferroelectric layer, we obtain SEM images and conduct XRD studies from poled and unpoled PVDF-TrFE films. To obtain a better signal-to-noise ratio, the sample thickness for the XRD measurements is higher than what is used in FETs. The PVDF-TrFE films are deposited on Si^{++} with thickness ∼800 nm.

D. Structure and morphology of PVDF-TrFE

Figures 5(a)–5(c) show the SEM images from unpoled, V-poled, and L-poled PVDF-TrFE films. The L-poled sample is the same one as the V-poled film; a lateral field of $\sim 10^5$ V/m is applied after obtaining the electron micrographs from the V-poled film. We note that the images are obtained with a low accelerating voltage of the electron beam and *in situ* nitrogen plasma cleaning of the thin-film surface in order to avoid any radiation damage or surface contamination due to residual hydrocarbons. Upon V-poling, the microstructure is seen to change compared to the unpoled sample; clear domains >1 μm are seen to form. Upon L-poling the same (V-poled) sample, the large domains are seen to diminish and the sample morphology becomes similar to the unpoled sample. These results indicate that a much smaller electric field in the lateral direction compared to the electric field in the vertical direction affects the microstructure, which most likely changes the ferroelectric domains.

Figure 5(d) shows the XRD data from unpoled, V-poled, and L-poled PVDF-TrFE films. In each case, the Si background is subtracted. The absolute intensities in Fig. 5(d) for the three samples are comparable as the thicknesses are similar. The poling condition for the L-poled film is similar to that used in Fig. 2(b), where the film is heated along with the application of a lateral field of $\sim 10^5$ V/m. The V-poled film is further L-poled using the same condition as in FETs. The XRD data from the same film for these two poling conditions are shown in the inset. The peak at 2θ of ∼20° is due to the 200 or 110 reflections, revealing the β phase structure [57]. The (hkl) indexing of (001) and (400/220) of the XRD Bragg peaks in Fig. 5(d) is based on the pseudohexagonal nature of the ferroelectric (FE) phase [58]. The V-poled sample shows the strongest intensity for the 200 or 110 reflection, suggesting an enhancement of the overall β phase. The L-poled and unpoled samples are almost identical except for a shoulder peak at ∼19°, which is more pronounced for the L-poled sample. This shoulder is most likely a signature of the α and γ phases of the paraelectric (PE) phase [59]; the deconvolution of the spectrum as two Gaussian peaks is shown in the inset.

The enhanced intensity of the β phase diffraction in PVDF-TrFE upon V-poling may be understood from previous XRD measurements in PVDF. The increase in polarization of a PVDF film (upon poling) originates from reorientation of the dipoles in the crystalline phase by an electric field rather than orientation of the dipoles of the amorphous (PE) phase [60–62]. It is pointed out that although the β phase unit cell is orthorhombic, it is very close to being hexagonal [24]. A small distortion of the primitive hexagonal unit cell is required to yield the β

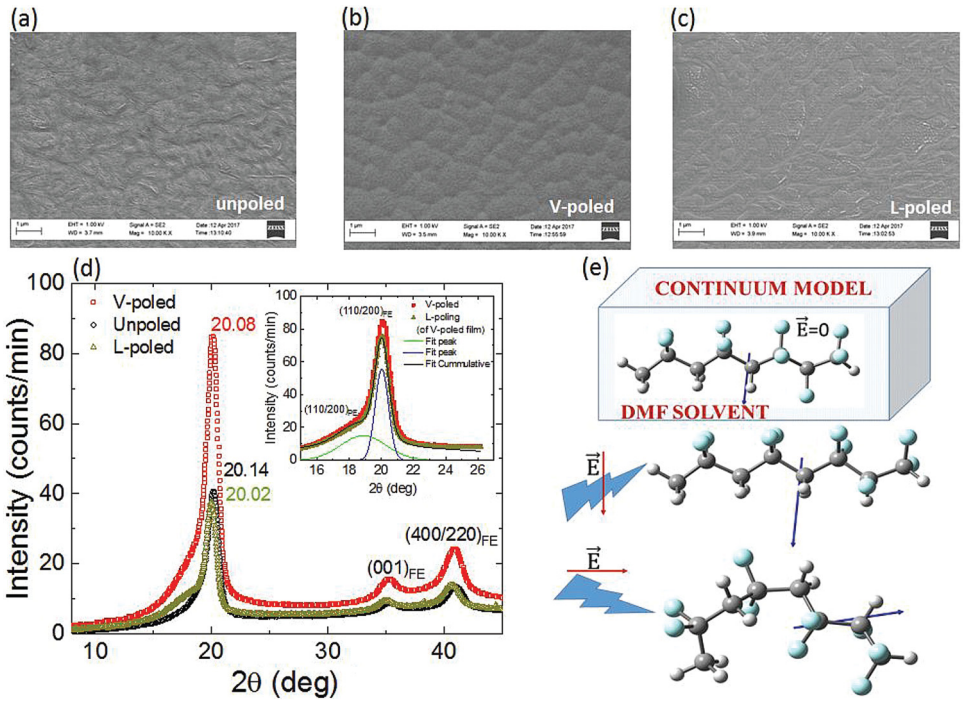

FIG. 5. Structure and morphology of PVDF-TrFE as a function of poling. (a)–(c) Scanning electron micrographs from unpoled, V-poled, and laterally L-poled films. (d) Grazing-incidence XRD from unpoled, V-poled, and L-poled PVDF-TrFE films on Si substrate. The (hkl) indexing is based on the ferroelectric phase as discussed in the text. The inset shows the XRD from the V-poled film and after L-poling the same V-poled film. Deconvolution of two peaks at 2θ (deg) (β phase) and at 18° for the paraelectric phase (PE) are shown for the laterally poled film. (e) Density-functional-theoretical calculations of the structural changes on a PVDF-TrFE oligomer enclosed in a dielectric medium upon the application of an external electric field. The color coding of the atoms is the same as in Fig. 1. Blue arrows indicate the direction of the dipole moment.

phase unit cell. A slight change in the peak position of the 200 or 110 reflection (of the β phase) upon V-poling compared to the unpoled sample in Fig. 5(d) may reflect a unit cell closer to the β phase unit cell. Due to the overlapping reflections, it is difficult to predict the exact lattice constants from our experiments.

Since the sample thickness of PVDF-TrFE for XRD measurements is about eight times more than those used in FETs, the polarization changes for the L-poled sample may even be higher in the FET devices compared to what is observed in Fig. 5(d). A small change in the XRD intensity after L-poling the V-poled film (in the inset) reflects a reorientation of the dipole moment of the unit cell that affects the β phase. However, this change is much smaller compared to the L-poled film, which is poled during recrystallization. Similar to the XRD results, the FET results show a larger difference in SS for the PVDF-TrFE film, which is L-poled during recrystallization compared to L-poling a V-poled FET (Tables I and II).

A simple molecular model is used to understand the role of the electric field on the dipole moment of a PVDF-TrFE molecule. Although in the crystalline environment, the mechanism of polarization rotation may be quite different, application of external fields to the molecule reveals changes in the all-*trans* configuration. As shown in Fig. 5(e), a single unit of the molecule is first optimized in a solvent bath. Since fluorine is more electronegative than hydrogen and carbon, the dipole moment points away from fluorine towards the hydrogen atoms (blue arrow). Electric fields of different magnitudes are applied in a perpendicular direction. Since the molecule is embedded in a solvent, the magnitude of the field in the DFT simulations is a few orders of magnitude higher compared to experiment. The dipole moment increases from 10 D (at zero external field) to almost 13 D after applying a maximum field of 3×10^9 V/m (Table S1 [42]). Applying a lateral field reorients the dipole moment in the horizontal direction and results in an overall buckling of the molecule [Fig. 5(e)] with a deviation from the all-*trans* phase. To mimic the reversal of the field in FET measurements, we reverse the direction of the applied lateral field. The molecule becomes linear but it does not recover to its initial all-*trans* phase (for the magnitude of the field shown).

These model calculations serve as a guide to correlate the changes in FET properties upon V- and L-poling for different magnitudes of applied fields. Application of a lateral electric field to the PVDF-TrFE film reorients the polarization in the horizontal direction such that it diminishes the screening charge accumulation, increasing SS and degrading FET properties. The simulations show that electric fields smaller by an order of magnitude in the lateral direction compared to the vertical direction can dramatically change the dipole moment (Fig. S12 [42]). This result is similar to our experimental observation where a lateral field, which is two or three orders of magnitude

smaller compared to the vertical field, can change SS by almost 40%.

IV. CONCLUSIONS

This work is a proof-of-concept that FET properties may be modulated by polarization rotation of the ferroelectric dielectric layer. Such an external tuning knob not only benefits an understanding of charge-transport mechanisms in a wide range of polymeric and molecular semiconductor-based devices but also provides new design architectures for improving FET performance. By employing low-operating voltage FETs, we independently exploit the impact of polarization rotation on the FET characteristics. A caveat for high-operating voltage FETs is that L-poled FETs may behave like V-poled devices due to polarization inversion in the dielectric layer by the gate voltage during normal FET operation.

A strong effect of polarization modulation may be envisioned if the transistor architecture is scaled down by reducing channel lengths, decreasing the distance between the lateral electrodes, and by using thin ferroelectric dielectric films. Channel lengths in the tens to hundreds of nm range and a thin dielectric layer (tens of nm) lowers the operating voltage of FETs. Such dimensions may allow poling of the dielectric layer during the normal operation of the FET, resulting in SS values close to that of MOSFETs. A small channel length, which may be achieved by nanolithography, allows the placement of the lateral electrodes closer than the mm distances used in this work. The energy needed for polarization rotation will thus be reduced, and one may expect larger differences in SS and other FET transport properties between V-poled and L-poled devices.

In summary, polarization rotation in a relaxor ferroelectric dielectric, PVDF-TrFE, has a profound effect on the transport properties of organic FETs. The subthreshold swing decreases and the overall FET properties are enhanced when the ferroelectric layer is vertically poled. The direction of polarization for the V-poled PVDF-TrFE film is chosen such that it is in the same direction as the gate electric field, enhancing charge accumulation in the channel region. Irrespective of the organic semiconductor, our results show that polarization orientation in the polymer ferroelectric layer directly controls SS and other FET parameters. Orienting and reorienting the polarization direction serves as a tuning parameter for manipulating SS and carrier mobilities in organic FETs. L-poling of a V-poled PVDF-TrFE film shows changes in carrier transport in FETs as well as reduces the overall capacitance in MIM structures. SEM images and XRD from poled and unpoled PVDF-TrFE reveal subtle changes in the microstructure and overall polarization of the PVDF-TrFE film. DFT calculations of the dipole moment from a molecular unit embedded in a solvent bath show anisotropy in the poling direction; a smaller electric field in the lateral direction (along the backbone of the molecule) compared to the perpendicular direction results in a large change in the dipole moment. This study highlights new design principles for organic FETs in lowering SS and enhancing transport properties by orienting the polarization direction in the ferroelectric dielectric layer.

ACKNOWLEDGMENTS

We acknowledge the support of this work through the National Science Foundation under Grant No. ECCS-1707588. P.F.M. and A.R.M. also acknowledge support from the NSF under Grant No. DGE-1069091. S.G. thanks the University of Missouri South African Education Program for travel funds to the U. Western Cape.

[1] J. Park, M. Kim, Y. Lee, H. S. Lee, and H. Ko, Fingertip skin-inspired microstructured ferroelectric skins discriminate static/dynamic pressure and temperature stimuli, Sci. Adv. **1**, e1500661 (2015).

[2] Prateek, V. K. Thakur, and R. K. Gupta, Recent progress on ferroelectric polymer-based nanocomposites for high energy density capacitors: Synthesis, dielectric properties, and future aspects, Chem. Rev. **116**, 4260 (2016).

[3] S. Horiuchi and Y. Tokura, Organic ferroelectrics, Nat. Mater. **7**, 357 (2008).

[4] R. C. G. Naber, C. Tanase, P. W. M. Blom, G. H. Gelinck, A. W. Marsman, F. J. Touwslager, S. Setayesh, and D. M. De Leeuw, High-performance solution-processed polymer ferroelectric field-effect transistors, Nat. Mater. **4**, 243 (2005).

[5] J. Hoffman, X. Pan, J. W. Reiner, F. J. Walker, J. P. Han, C. H. Ahn, and T. P. Ma, Ferroelectric field effect transistors for memory applications, Adv. Mater. **22**, 2957 (2010).

[6] S. J. Kang, Y. J. Park, I. Bae, K. J. Kim, H-C. Kim, S. Bauer, E. L. Thomas, and C. Park, Printable ferroelectric pvdf/pmma blend films with ultralow roughness for low voltage non-volatile polymer memory, Adv. Funct. Mater. **19**, 2812 (2009).

[7] J.-H. Lee, H.-J. Yoon, T. Y. Kim, M. K. Gupta, J. H. Lee, W. Seung, H. Ryu, and S.-W. Kim, Micropatterned p(vdf-trfe) film-based piezoelectric nanogenerators for highly sensitive self-powered pressure sensors, Adv. Funct. Mater. **25**, 3203 (2015).

[8] M. Zirkl, A. Sawatdee, U. Helbig, M. Krause, G. Scheipl, E. Kraker, P. A. Ersman, D. Nilsson, D. Platt, P. Bodö, S. Bauer, G. Domann, and B. Stadlober, An all-printed ferroelectric active matrix sensor network based on only five functional materials forming a touchless control interface, Adv. Mater. **23**, 2069 (2011).

[9] Y. Yuan, T. J. Reece, P. Sharma, S. Poddar, S. Ducharme, A. Gruverman, Y. Yang, and J. Huang, Efficiency enhancement in organic solar cells with ferroelectric polymers, Nat. Mater. **10**, 296 (2011).

[10] R. C. G. Naber, M. Mulder, B. De Boer, P. W. M. Blom, and D. M. De Leeuw, High charge density and mobility in

poly(3-hexylthiophene) using a polarizable gate dielectric, Org. Electron. **7**, 132 (2006).

[11] J. J. Brondijk, K. Asadi, P. W. M. Blom, and D. M. De Leeuw, Physics of organic ferroelectric field-effect transistors, J. Polym. Sci. Part B Polym. Phys. **50**, 47 (2012).

[12] G. Knotts, A. Bhaumik, K. Ghosh, and S. Guha, Enhanced performance of ferroelectric-based all organic capacitors and transistors through choice of solvent, Appl. Phys. Lett. **104**, 233301 (2014).

[13] C. A. Nguyen, S. G. Mhaisalkar, J. Ma, and P. S. Lee, Enhanced organic ferroelectric field effect transistor characteristics with strained poly(vinylidene fluoride-trifluoroethylene) dielectric, Org. Electron. **9**, 1087 (2008).

[14] I. N. Hulea, S. Fratini, H. Xie, C. L. Mulder, N. N. Iossad, G. Rastelli, S. Ciuchi, and A. F. Morpurgo, Tunable Fröhlich polarons in organic single-crystal transistors, Nat. Mater. **5**, 982 (2006).

[15] S. J. Konezny, M. N. Bussac, and L. Zuppiroli, Hopping and trapping mechanisms in organic field-effect transistors, Phys. Rev. B **81**, 045313 (2010).

[16] Y. Mei, P. J. Diemer, M. R. Niazi, R. K. Hallani, K. Jarolimek, C. S. Day, C. Risko, J. E. Anthony, A. Amassian, and O. D. Jurchescu, Crossover from band-like to thermally activated charge transport in organic transistors due to strain-induced traps, Proc. Natl. Acad. Sci. **114**, E6739 (2017).

[17] H. Kimura, T. Hanyu, M. Kameyama, Y. Fujimori, T. Nakamura, and H. Takasu, Complementary ferroelectric-capacitor logic for low-power logic-in-memory VLSI, IEEE J. Solid-State Circuits **39**, 919 (2004).

[18] S. Sakai and M. Takahashi, Recent advances in ferroelectric-gate field-effect-transistor technology, Integr. Ferroelectr. **124**, 140 (2011).

[19] S. Mathews, R. Ramesh, T. Venkatesan, and J. Benedetto, Ferroelectric field effect transistor based on epitaxial perovskite heterostructures, Science **276**, 238 (1997).

[20] H. Fu and R. E. Cohen, Polarization rotation mechanism for ultrahigh electromechanical response in single-crystal piezoelectrics, Nature **403**, 281 (2000).

[21] V. Nagarajan, A. Roytburd, A. Stanishevsky, S. Prasertchoung, T. Zhao, L. Chen, J. Melngailis, O. Auciello, and R. Ramesh, Dynamics of ferroelastic domains in ferroelectric thin films, Nat. Mater. **2**, 43 (2003).

[22] J. Hlinka and P. Marton, Phenomenological model of a 900 domain wall in $BaTiO_3$-type ferroelectrics, Phys. Rev. B **74**, 104104 (2006).

[23] H. Kawai, The piezoelectricity of poly (vinylidene fluoride), Jpn. J. Appl. Phys. **8**, 975 (1969).

[24] R. G. Kepler and R. A. Anderson, Ferroelectricity in polyvinylidene fluoride, J. Appl. Phys. **49**, 1232 (1978).

[25] A. J. Lovinger, Ferroelectric polymers, Science **220**, 1115 (1983).

[26] A. J. Lovinger, D. D. Davis, R. E. Cais, and J. M. Kometani, On the Curie temperature of poly(vinylidene fluoride), Macromolecules **19**, 1491 (1986).

[27] T. Furukawa, Piezoelectricity and pyroelectricity in polymers, IEEE Trans. Electr. Insul. **24**, 375 (1989a).

[28] J. Zaumseil and H. Sirringhaus, Electron and ambipolar transport in organic field-effect transistors, Chem. Rev. **107**, 1296 (2007).

[29] S. P. Senanayak, S. Guha, and K. S. Narayan, Polarization fluctuation dominated electrical transport processes of polymer-based ferroelectric field effect transistors, Phys. Rev. B **85**, 115311 (2012).

[30] A. Laudari and S. Guha, Polarization-induced transport in ferroelectric organic field-effect transistors, J. Appl. Phys. **117**, 105501 (2015).

[31] A. Laudari and S. Guha, Bandlike Transport in Ferroelectric-Based Organic Field-Effect Transistors, Phys. Rev. Appl. **6**, 044007 (2016).

[32] J. Li, D. Taguchi, W. OuYang, T. Manaka, and M. Iwamoto, Interaction of interfacial charge and ferroelectric polarization in a pentacene/poly(vinylidene fluoride-trifluoroethylene) double-layer device, Appl. Phys. Lett. **99**, 063302 (2011).

[33] T. Otsuka, D. Taguchi, T. Manaka, and M. Iwamoto, Direct visualization of polarization reversal of organic ferroelectric memory transistor by using charge modulated reflectance imaging, J. Appl. Phys. **122**, 185501 (2017).

[34] S. P. Senanayak and K. S. Narayan, Strategies for fast-switching in all-polymer field effect transistors, Adv. Funct. Mater. **24**, 3324 (2014).

[35] A. Z. Ashar and K. S. Narayan, Electric field induced ferroelectric-surface modification for high mobility organic field effect transistors, Org. Electron. **42**, 8 (2017).

[36] Y. Qi and A. M. Rappe, Designing Ferroelectric Field-Effect Transistors Based on the Polarization-Rotation Effect for Low Operating Voltage and Fast Switching, Phys. Rev. Appl. **4**, 044014 (2015).

[37] U. Zschieschang, V. P. Bader, and H. Klauk, Below-one-volt organic thin-film transistors with large on/off current ratios, Org. Electron. **49**, 179 (2017).

[38] U. Zschieschang and H. Klauk, Low-voltage organic transistors with steep subthreshold slope fabricated on commercially available paper, Org. Electron. **25**, 340 (2015).

[39] B. Blülle, R. Häusermann, and B. Batlogg, Approaching the Trap-Free Limit in Organic Single-Crystal Field-Effect Transistors, Phys. Rev. Appl. **1**, 034006 (2014).

[40] I. Katsouras, D. Zhao, M.-J. Spijkman, M. Li, P. W. M. Blom, D. M. de Leeuw, and K. Asadi, Controlling the on/off current ratio of ferroelectric field-effect transistors, Sci. Rep. **5**, 12094 (2015).

[41] C. Bourgaux-Leonard, J. F. Legrand, A. Renault, and P. Delzenne, Annealing effects in ferroelectric poly(vinylidene fluoride-trifluoroethylene) copolymers: real-time studies using synchrotron radiation, Polymer **32**, 597 (1991).

[42] See Supplemental Material at https://link.aps.org/supplemental/10.1103/PhysRevApplied.10.014011 for a schematic and image of FET devices; FET output and MIS characteristics of DNTT-based devices; Transfer characteristics of DNTT FETs in double linear plots; Contact resistance; Electrical characteristics of pentacene and TIPS-pentacene FETs; Interfacial potential of DNTT FETs; Typical FET characteristics of DNTT-based devices with a 30 nm PVDF-TrFE layer; Capacitance characteristics from 30 nm PVDF-TrFE MIM capacitors; DFT optimization of a

PVDF-TrFE molecule in a solvent atmosphere; Theoretical structural changes of a PVDF-TrFE molecule after the application of a lateral electric field; Dipole moment of a PVDF-TrFE (in a solvent bath) upon application of an external electric field in the perpendicular direction.

[43] Gaussian09, "Gaussian 09, revision b.01, gaussian, inc., wallingford, ct," Revision B.01, Gaussian, Inc., Wallingford, CT (2009).

[44] T. Furukawa, Ferroelectric properties of vinylidene fluoride copolymers, Phase Transitions **18**, 143 (1989b).

[45] T. Putzeys and M. Wubbenhorst, Asymmetric polarization and hysteresis behaviour in ferroelectric P(VDF-TrFE) (76 : 24) copolymer thin films spatially resolved via limm, Phys. Chem. Chem. Phys. **17**, 7767 (2015).

[46] U. Zschieschang, F. Ante, D. Kälblein, T. Yamamoto, K. Takimiya, H. Kuwabara, M. Ikeda, T. Sekitani, T. Someya, J. B. Nimoth, and H. Klauk, Dinaphtho[2,3-b:2′,3′-f]thieno[3,2-b]thiophene (dntt) thin-film transistors with improved performance and stability, Org. Electron. **12**, 1370 (2011).

[47] H. H. Choi, K. Cho, C. D. Frisbie, H. Sirringhaus, and V. Podzorov, Critical assessment of charge mobility extraction in FETs, Nat. Mater. **17**, 2 (2018).

[48] V. Podzorov, S. E. Sysoev, E. Loginova, V. M. Pudalov, and M. E. Gershenson, Single-crystal organic field effect transistors with the hole mobility 8 $cm^2/V\,s$, Appl. Phys. Lett. **83**, 3504 (2003).

[49] D. J. Gundlach, L. Zhou, J. A. Nichols, T. N. Jackson, P. V. Necliudov, and M. S. Shur, An experimental study of contact effects in organic thin film transistors, J. Appl. Phys. **100**, 024509 (2006).

[50] F. Ante, D. Kälblein, T. Zaki, U. Zschieschang, K. Takimiya, M. Ikeda, T. Sekitani, T. Someya, J. N. Burghartz, K. Kern, and H. Klauk, Contact resistance and megahertz operation of aggressively scaled organic transistors, Small **8**, 73 (2012).

[51] E. G. Bittle, J. I. Basham, T. N. Jackson, O. D. Jurchescu, and D. J. Gundlach, Mobility overestimation due to gated contacts in organic field-effect transistors, Nat. Commun. **7**, 10908 (2016).

[52] M. Grünewald, P. Thomas, and D. Würtz, A simple scheme for evaluating field effect data, Physica Status Solidi (b) **100**, K139 (1980).

[53] L. Kalb Wolfgang and Batlogg Bertram, Calculating the trap density of states in organic field-effect transistors from experiment: A comparison of different methods, Phys. Rev. B **81**, 035327 (2010).

[54] P. J. Diemer, Z. A. Lamport, Y. Me, J. W. Ward, K. P. Goetz, W. Li, M. M. Payne, M. Guthold, J. E. Anthony, and O. D. Jurchescu, Quantitative analysis of the density of trap states at the semiconductor-dielectric interface in organic field-effect transistors, Appl. Phys. Lett. **107**, 103303 (2015).

[55] S.-W. Jung, K.-J. Baeg, S.-M. Yoon, I.-K. You, J.-K. Lee, Y.-S. Kim, and Y.-Y. Noh, Low-voltage-operated top-gate polymer thin-film transistors with high capacitance poly(vinylidene fluoride-trifluoroethylene)/poly(methyl methacrylate) dielectrics, J. Appl. Phys. **108**, 102810 (2010).

[56] H. Sun, Q. Wang, Y. Li, Y.-F. Lin, Y. Wang, Y. Yin, Y. Xu, C. Liu, K. Tsukagoshi, L. Pan, X. Wang, Z. Hu, and Y. Shi, Boost up carrier mobility for ferroelectric organic transistor memory via buffering interfacial polarization fluctuation, Sci. Rep. **4**, 7227 (2014).

[57] D. Guo, and N. Setter, Impact of confinement-induced cooperative molecular orientation change on the ferroelectric size effect in ultrathin P(VDF-TrFE) films, Macromolecules **46**, 1883 (2013).

[58] M.-C. Garcia-Gutierrez, A. Linares, I. Martin-Fabiani, J. J. Hernandez, M. Soccio, D. R. Rueda, T. A. Ezquerra, and M. Reynolds, Understanding crystallization features of P(VDF-TrFE) copolymers under confinement to optimize ferroelectricity in nanostructures, Nanoscale **5**, 6006 (2013).

[59] P. Martins, A. C. Lopes, and S. Lanceros-Mendez, Electroactive phases of poly(vinylidene fluoride): Determination, processing and applications, Prog. Polym. Sci. **39**, 683 (2014).

[60] G. A. Samara, "Ferroelectricity revisited-advances in materials and physics," Solid State Physics, Vol. 56, edited by Henry Ehrenreich and Frans Spaepen (Academic Press, 2001) pp. 239–458.

[61] R. G. Kepler and R. A. Anderson, Ferroelectric polymers, Adv. Phys. **41**, 1 (1992).

[62] H. Dvey-Aharon, T. J. Sluckin, P. L. Taylor, and A. J. Hopfinger, Kink propagation as a model for poling in poly(vinylidene fluoride), Phys. Rev. B **21**, 3700 (1980).